Applied Energy 295 (2021) 117062

Contents lists available at ScienceDirect

Applied Energy

journal homepage: www.elsevier.com/locate/apenergy

Energy management for an electro-thermal renewable–based residential microgrid with energy balance forecasting and demand side management

Julio Pascual [a,*], Diego Arcos-Aviles [b], Alfredo Ursúa [a], Pablo Sanchis [a], Luis Marroyo [a]

[a] Department of Electrical, Electronic and Communications Engineering, Institute of Smart Cities, Public University of Navarre (UPNA), Edificio de los Pinos, Campus Arrosadía s/n, 31006 Pamplona, Spain
[b] Departamento de Eléctrica y Electrónica, Grupo de investigación PROCONET, Universidad de las Fuerzas Armadas ESPE, Av. Gral. Rumiñahui s/n, 171-5-231B, Sangolquí, Ecuador

HIGHLIGHTS

- Energy management strategy for a renewable-based electro-thermal microgrid.
- Minimize power peaks and fluctuations in the grid using power forecasting.
- Using two systems of energy storage (heat and battery) and demand side management.
- Analysis by means of simulation has been carried out using one-year measured data.
- Experimental validation has been done in a real size microgrid.

GRAPHICAL ABSTRACT

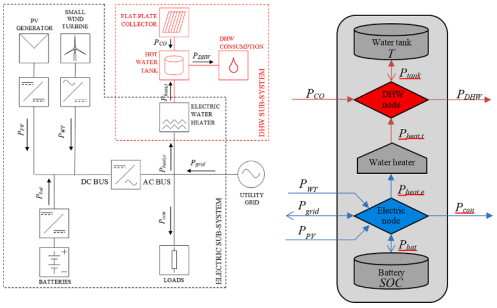

ARTICLE INFO

Keywords:
Microgrids
Renewable energy
Energy management
Energy storage
Forecasting
Demand side management

ABSTRACT

This paper proposes an energy management strategy for a residential microgrid comprising photovoltaic (PV) panels, a small wind turbine and solar thermal collectors. The microgrid can control the power exchanged with the grid thanks to a battery and a controllable electric water heater, which provide two degrees of freedom to the control strategy. As input data, the proposed control strategy uses the battery state of charge (SOC), the temperature of the hot water tank, the power of each microgrid element as well as the demand and renewable generation forecasts. By using forecasted data and by controlling the electric water heater, the strategy is able to achieve a better grid power profile while using a smaller battery than previous works, hence reducing the overall cost of the system. The strategy is tested by means of simulation with real data for one year and it is also experimentally validated in the microgrid built at the Renewable Energy Laboratory at the UPNA.

1. Introduction

There is general agreement in that renewable energies, especially wind and photovoltaic (PV) power, are set to increase their share in the global energy mix so as to become two of the largest energy sources in electricity generation in the near future [1]. However, there are two main challenges to the high penetration level of such energy sources in the system. On one hand, there is the need of an energy reservoir during long periods due to the intermittent nature of wind and solar energy,

* Corresponding author.
E-mail address: juliomaria.pascual@unavarra.es (J. Pascual).

https://doi.org/10.1016/j.apenergy.2021.117062
Received 26 November 2020; Received in revised form 12 April 2021; Accepted 3 May 2021
Available online 13 May 2021

Nomenclature

FE	Integrated forecasting error of P_{bal} in the previous 3 h
K_{24}	Parameter to calculate P_{SOC24} in Step 2 of the proposed strategy
K_{P1}	Control variable used in Step 2 of the proposed strategy.
$K_{P1,\max}$	Maximum value of functions $K_{P1,neg}$ and $K_{P1,pos}$
$K_{P1,neg}$	Control function used in Step 2 if the forecasting error is negative
$K_{P1,pos}$	Control function used in Step 2 if the forecasting error is positive
K_{P2}	Control variable used in Step 2 of the proposed strategy as a function of FE
K_T	Parameter to calculate P_{T24} in Step 3 of the proposed strategy
P_{bal}	Balance of the power flows through the boundary of the microgrid excluding P_{grid}
$P_{bal,CMA}$	24-h central moving average of P_{bal}
$P_{bal,fore}$	Forecasted value of P_{bal}
$P_{bal,t}$	Power balance of the power variables in the thermal node excluding $P_{heat,t}$
$P_{bal,t,CMA}$	24-hour central moving average of $P_{bal,t}$
P_{bat}	Battery flowing from the battery into the electric node
$P_{bat,1}$	Preliminary value of the battery power used within Step 5 of the proposed strategy
P_{CO}	Power output of the solar thermal collectors
P_{con}	Power consumption of the non-manageable loads, i.e., excluding $P_{heat,e}$
P_{DHW}	DHW power consumption
P_{grid}	Power coming from the grid into the microgrid
$P_{grid,1}$	Preliminary value of the grid power calculated in Step 1 of the proposed strategy
$P_{grid,2}$	Preliminary value of the grid power calculated in Step 2 of the proposed strategy
$P_{heat,e}$	Electric input power of the water heater
$P_{heat,e,1}$	Preliminary value of the electric power of the water heater calculated in Step 3 of the proposed strategy
$P_{heat,e,2}$	Preliminary value of the electric power of the water heater calculated in Step 4 of the proposed strategy
$P_{heat,t}$	Thermal output power of the water heater
P_{min}	Parameter that defines the maximum power to be fed into the grid, i.e., minimum power to be exchanged with the grid
P_{net}	Power balance of the electric node excluding P_{grid}
P_{PV}	Photovoltaic power
P_{SOC}	Power component of $P_{grid,2}$ used in Step 2 of the proposed strategy depending on the SOC and FE
P_{SOC24}	Power component of $P_{grid,2}$ used in Step 2 of the proposed strategy depending on SOC_{24h}
P_{T24}	Power component of $P_{heat,e,1}$ in Step 3 of the proposed strategy
P_{WT}	Wind turbine power
$refSOC$	Reference setpoinf for the SOC of the battery
SOC	State of charge of the battery
SOC_{24h}	24-h simple moving average of SOC
T	Temperature of the water in the water tank
T_{24h}	24-h simple moving average of T

which is to be solved by a combination of technologies and techniques, mainly energy storage, complementary power sources or demand-side management. On the other hand, even if energy needs are met, as synchronous generators are being substituted by electronic converters, a lack of inertia may compromise the stability of the grid; this may be solved by having a certain percentage of synchronous generators running or including virtual inertia in the control of power converters that drive both the energy generators or storage.

Integrating all these solutions for every power unit in the grid would be quite a complex task. This can be partly solved by clustering these individual units into microgrids [2], where power sources, energy storage systems, demand-side management, etc. are controlled locally while keeping an only point of common coupling with the grid. This solution may alleviate the grid control and stability while optimizing its energy management, including thermal loads, resulting in lower operating costs as seen in [3].

For this reason, microgrids are becoming a promising alternative to traditional centralized electric systems both in technologically advanced countries and developing ones [4–6]. Microgrids, as defined in [7], comprise manageable loads, distributed generation, energy storage, and are managed as a single unit in order to exchange power with the grid through a single coupling point. As a result, there are many possible configurations, each with its own energy management strategy.

The energy management strategy is responsible of setting the operating point of every manageable unit in a microgrid, which will be different depending on the goal of the strategy and its performance. A comprehensive review of some of the latest papers regarding microgrids' energy management can be found in [8]. Some of these papers focus on minimizing the overall operating cost based on the cost of operation of every unit as well as the market electricity price [9–15]. A new interesting trend consists on the management of several microgrids under one only supervisory system. This multimicrogrid systems permit to, not only minimize operating costs of every microgrid, but also to take into account the grid needs, e.g., three-phase power balancing [16] or energy reserve in order to respond to outages or unpredicted renewable variations [17,18], i.e., ancillary services through energy storage or demand response programs such as those in [19].

Nevertheless, market electricity prices in well regulated markets depend on technical issues, mainly, the primary source for generating electricity, which, in part, may depend on the saturation of the transmission system or the availability of renewable power. For this reason, the strategy hereby presented focuses on balancing energy generation and consumption locally by using energy storage and manageable loads, with the goal of reducing generation and consumption peaks in the power profile exchanged with the grid. Additionally, grid power fluctuations are reduced by making use of the energy storage system. By focusing on this technical aspects, similarly to [20–27], the strategy results in the following outcomes: (1) reduction of overvoltage events in low-voltage grids when power is injected into the main grid, [28,29]; (2) saturation alleviation in transmission lines [30]; and (3) reduction in power fluctuations which leads to better grid quality and stability [31,32]. These outcomes are necessary for further integration of renewables in low-voltage grids, if quality and stability of grid are to be maintained or even enhanced. However, this is done at the expense of adding storage elements that must be minimized in order to reduce costs. Hence, the strategy proposed helps passively with the grid operation while minimizing the battery needed. Moreover, note that, although not considered in this paper, ancillary services or integration of the system in multimicrogrid systems would be compatible with this strategy.

A simple practical way to reduce power peaks and fluctuations in the power exchanged with the grid is to apply a low pass filter to the power balance profile inside the microgrid, separating its low and high frequencies and letting the grid to deliver only the lower frequencies by making a battery to deliver the higher frequencies [20,21]. This can be simply achieved by implementing a simple moving average (SMA) filter,

which is a usual benchmark and is used as one of the comparison scenarios in this study. However, the SMA strategy results in a greater need of battery capacity than other state-of-the-art strategies, partly due to the lag introduced by such filter. In the case study used as an example in this paper, a 60 kWh battery would be needed should this strategy be used, which represents 5 h of storage relative to the renewable generators. This is an unpractical size for a residential microgrid, partly due to its physical size but, more importantly, due to its high cost, which, in fact, is one of the main barriers against the integration of high shares of renewables in the grid or in microgrids.

In order to reduce the battery capacity needed, a more sophisticated energy management strategy than the SMA-based was presented in [23], which proposed an algorithm to calculate the power exchanged with the grid by using linear programming dependent on the SOC of the battery and the power generated and consumed by every unit in the microgrid. This approach led to a reduction of the battery capacity of 25%, down to 45 kWh. A similar approach was carried out in [24] and [33] using this time fuzzy logic control. However, the grid power in all these approaches presented some undesired peaks and fluctuations when the battery was fully charged or depleted.

In order to enhance the grid power profile seen in [23] while maintaining the battery size, the strategy was upgraded in [25] by integrating the thermal part of the microgrid in the energy management system which is of great help for managing the power system as also seen in [29,34] at a better cost than batteries as analyzed in [35]. This is mainly due to these three characteristics of the thermal system in a building: (1) it comprises controllable high-power devices; (2) it usually handles a big fraction of the energy used in microgrids; and (3) it usually provides extra energy storage in the form of a hot water tank or other forms of heat or cold storage. Following this idea, in the case study of [23], the controller now manages the electric heater of the domestic hot water (DHW) system in order to enhance the use of the 45 kWh battery taking advantage of the hot water tank ability to store energy. The grid power profile was satisfactorily smoothed by using such demand-side management technique. This conclusion was also true when using a fuzzy logic controller as shown in [36], which suggests the importance of integrating the thermal subsystem of a microgrid in the energy management.

In [37], in order to further reduce the battery size, the moving average approach was brought back but, this time, the strategy was based on the central moving average (CMA) in order to avoid the lag introduced by the SMA in the grid power profile, which was responsible of large SOC swings. Nevertheless, such strategy needs forecasted values for the power profiles in the microgrid, which are calculated using weather forecasting for renewable generation, and persistence techniques for demand profiles. The forecasting error was introduced as a new variable for the SOC control. This new approach permitted a further reduction of the battery size, down to 36 kWh, while maintaining a similar grid power profile than in [23]. The philosophy of control used in [37] was also programmed using fuzzy logic as presented in [38,39]. Note that, unlike [23] neither of these CMA-based strategies make use of the thermal subsystem of the microgrid for the control of the grid power.

In this paper, we have designed a new strategy based on the CMA approach in [37] and the use of the electric water heater for demand side management as in [23], so that the battery can be further reduced by 25%, down to 27 kWh, yet achieving a similar power profile than in [37]. Bringing an extra degree of freedom, in order to integrate the thermal part, a new strategy is proposed which comprises two main stages. The first stage is aimed at maintaining the energy balance of the microgrid by calculating the energy to be imported from the grid, based on the rest of energy flows coming in and out of the system and their predicted values for the following 12 h. In the second stage, a similar approach is taken but only for the thermal subsystem. Given the flexibility of the electric water heater, which can be operated at any power level between zero up to its rated power, this second stage features some additional demand-side management techniques. The electric power heater can not only be used to provide the energy demanded by the DHW system with a smooth power profile, but it can also absorb surplus energy from the generators that would otherwise be injected into the grid or into the battery, which could be undesirable at certain moments. In other words, the control of the water heater, based on the prediction of thermal energy flows and the state of charge of the energy storage elements (hot water tank and the battery) permits to absorb power peaks from the generators and to help with the battery SOC control by heating the water in the hot water tank whenever the SOC of the battery tends to a full charge. In this way, the SOC of the battery may be kept under 90% leaving a capacity margin in order to absorb power peaks whenever the hot water tank may not be able to absorb that extra energy, i.e., whenever it has reached its maximum temperature. In this way, not only the grid power profile may be enhanced in terms of stability with respect to that in [37] but also, the resulting grid power profile is similar to the objective power profile, i.e. the SMA of the net power. More importantly, this is now achieved with a reduction of 25% in battery capacity with respect to [37] and a reduction of 55% with respect to the SMA strategy, which would result in a notable reduction of the cost of the microgrid. This is achieved thanks to both the integration of the thermal subsystem, and the forecasting of power profiles. Note that, as the thermal subsystem adds a new degree of freedom, a new strategy has been designed in order to integrate it in the energy management system, achieving similar results than previous strategies in terms of power profile but minimizing the battery size.

This is one of the most important points of this paper because, as renewable energies like wind and PV are integrated in the power system, more storage will be needed. These energy sources already provide energy at costs below nowadays market prices, but the storage required, generally in the form of batteries, will increase overall energy costs above nowadays market prices unless energy management strategies are designed so that they reduce the need of energy storage. The strategies proposed in the reviewed papers used a battery with a capacity between 36 and 60 kWh, i.e., an energy storage of 3 to 5 h with respect to wind plus PV generation (12 kW) which could more than double overall costs. In this paper, this value is reduced to 2,25 h, making this solution more affordable and even cheaper than market energy prices in certain regions [40].

To sum up, the work in this paper addresses most solutions generally adopted for the integration of high shares of renewable energies, including energy storage by means of both battery and thermal storage along with demand-side management and forecasting techniques. With the new energy management strategy, the battery capacity needed has been reduced by up to 55% while preserving a similar grid power profile than in previous works, hence, the overall cost of the system has been reduced. Moreover, the demand-side techniques used with this strategy do not affect the end-user experience as only the power of the water heater is modified, but always keeping the water temperature between usable limits. Although not considered in this work, the strategy is compatible with ancillary services. Also note that being a rule-based control, the strategy may be easily adapted for other microgrids. By means of simulation using a year of real data, this work quantifies and compares how this system performs when compared, under the same conditions, with other state-of-the-art strategies that use these techniques separately. Moreover, the proposed algorithm is validated experimentally in a microgrid testbed built at the Energy Storage and Microgrids Laboratory of UPNA.

From this point, the paper is organized as follows: in Section 2 the microgrid architecture is presented, the problem is analyzed and a set of quality criteria are defined in order to compare different strategies. In Section 3, the proposed strategy is explained and its simulation results are analyzed and compared with state of the art solutions. Section 4 presents the microgrid testbed and the experimental results. Finally, in Section 5, the main conclusions are discussed.

2. Microgrid architecture and formulation of the problem

Even though the strategy presented may be applied to several microgrid cases, in order to quantify the results obtained with different strategies, a particular case has been selected. This case study is based on that presented in [37], which consists of a single family house of which electric demand including space heating and cooling is considered, and that is able to provide up to 87% of its demand with an on-site PV system and a small wind turbine. The rest of the energy is taken from the grid in a controlled manner thanks to a battery. Apart from that, in this paper, the DHW demand is added which gets its energy partially from a solar thermal collector and a controllable electric water heater which permits to control the battery SOC and the grid power profile. A hot water tank is used as an energy buffer in order to decouple power flows in the DHW subsystem. Globally, this new electro-thermal microgrid can generate up to 80% of its demand with on-site renewables. The missing 20% is taken from the grid controlling the power flow so as to smooth the grid power profile, avoiding power peaks and fluctuations, which is the main objective of the proposed energy management strategy.

Fig. 1a shows the architecture of the power elements of the microgrid. As it can be observed, there are two differentiated areas, namely, the electric subsystem and the DHW subsystem. In the electric subsystem the battery (27 kWh), PV generator (6 kW) and wind turbine (6 kW) feed energy to the DC bus, which in turn is transferred to the AC bus with a bidirectional inverter. The loads are connected to the AC bus which is also connected to the grid. On the other hand, the DHW subsystem comprises a hot water tank (800 L) which feeds the house with hot water. This hot water tank gets the energy needed from solar thermal collectors (2 kW) and the controllable water heater (2 kW), which is the link between the electric and the DHW subsystems. This water electric heater and the water tank are, together with the battery, the elements that permit to control the power exchange with the grid. Note that the size of the elements used is the same as in previous works [25] and [37] so as to compare them under the same conditions; except for the battery, which is reduced using the new strategy. This sizing results in an 80% of the energy consumed in the microgrid being generated locally by renewable sources. The remaining 20% comes from the grid in a controlled way, reducing power peaks and fluctuations so as to alleviate the operation of the grid.

Fig. 1b shows eschematically the energy flows in the microgrid. As it can be seen, power entering the system is the power generated by the PV panels (P_{PV}), the wind turbine (P_{WT}), solar thermal collectors (P_{CO}) and the grid (P_{grid}). The power outputs are the DHW consumption (P_{DHW}) and the electric loads excluding the electric water heater (P_{con}). The electric water heater power flow represents neither an input nor an output to the microgrid, but it rather trasfers energy from the electric subsystem to the DHW subsystem. It can also be observed that, asuming that generators always are at their maximum power point, the only controllable (although indirectly) power entering or leaving the system is the power from the grid. Also note that, the way the system has been defined in Fig. 1b, the power balance both in the electric node and the thermal node is always zero. However, thanks to the storage systems, there is one degree of freedom in each of the nodes, which permit to adjust the grid power by controlling the power of both the battery and the electric water heater. Considering the convention of energy flows shown in Fig. 1b, the power exchanged with the grid at a certain instant can be calculated as follows:

$$P_{grid} = P_{con} + P_{heat,e} - P_{PV} - P_{WT} - P_{bat}. \quad (1)$$

Defining the net power as the addition of the power consumed by the electric loads (P_{con} and $P_{heat,e}$) minus the power generated by the local electric generators (P_{PV} and P_{WT}), the grid power can be expressed as the difference between P_{net} and P_{bat}:

$$P_{net} = P_{con} + P_{heat,e} - P_{PV} - P_{WT} \Rightarrow P_{grid} = P_{net} - P_{bat}. \quad (2)$$

The variables needed for this study have been measured with a 1-second sampling rate and during one year in a real two-storied, single-family home for the consumption profiles; and in the laboratory for the generation. Both the house and the laboratory are located in Pamplona, northern Spain. Note that the measured PV power profile has been linearly scaled up from 4 to 6 kW in order to reach the PV power of the case study. On the other hand, as $P_{heat,e}$ depends on the strategy, it has been

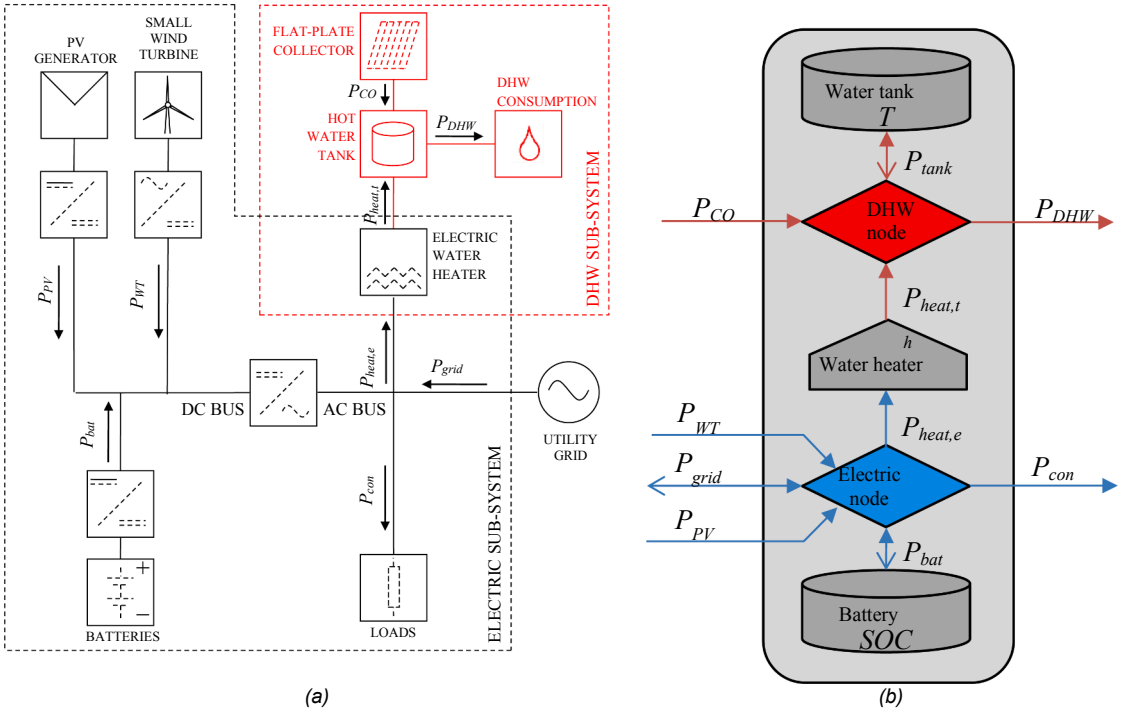

Fig. 1. Microgrid schematic and energy flows. Doubly ended arrows represent bidirectional energy flows, which are considered positive in the direction of the solid arrow.

calculated by simulation of the thermal system for every scenario.

Using these data, the proposed energy management strategy has been analyzed from the point of view of power management and from the point of view of the energy management of the battery. As such, on one hand, the ability of this strategy to compensate rapid power fluctuations has been proved by means of both simulation and experimental testing by running the strategy during nine days at a sampling rate of 1 s, as presented in Section 4. On the other hand, given that both consumption and renewable generation have a seasonal behavior, the strategy has also been tested during a year from the point of view of the control of the SOC of the battery. In order to speed up the 1-year simulations, a sampling rate of 15 min has been chosen, which can be done without affecting the results, as power fluctuations below this period will not have a significant effect in the SOC of the battery in this case study.

In order to compare the strategies' performance, a first reference case is used where there are no batteries and the water heater works under a hysteresis control to maintain the water between 50 °C and 55 °C. In this case, there are no degrees of freedom and the power exchanged with the grid is determined by the remaining power flows. From Eq. (2), as there is no battery ($P_{bat} = 0$), the power exchanged with the grid in this reference scenario, is equal to the net power (P_{net}).

The resulting yearly net power profile is shown in Fig. 2a, where it can be observed that maximum peak powers from and into the grid are around 6 kW. Moreover, as shown in Fig. 2.b, where 4 days of the net power profile are shown, steep power ramps occur every day which are greater than those of the power consumption itself. This is due to the coincidence of the ramp up of power demand in the evening and the ramp down of PV power at that same time. This typical pattern occurring in electric systems with high PV integration is one of the key aspects to overcome in the near future as seen in [41]. Nonetheless, the reason for using storage elements and so the objective of the energy management strategies is to smooth the power profile exchanged with the grid in terms of both power peaks and power ramps.

Given that major fluctuations occur on a daily basis, a power profile that shows low power peaks and ramps could be easily calculated as the 24 h SMA of the net power. As such, in this paper as well as in other works of the literature, this power profile is used as a benchmark. Obtaining this power profile only requires calculating the average of the last 24 h of the net power at every time step and assign it to the grid. In order to attain this, the difference between the net power and the averaged power has to be provided by the battery, as shown in Fig. 3.

Fig. 4a shows the power profile during a year resulting from averaging the net power using a 24 h window. Fig. 4b shows a close up of both the net power and the averaged power profile during the same 4 days shown in Fig. 2b. These figures show how power peaks and

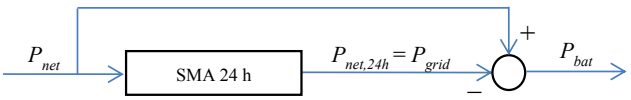

Fig. 3. Simple moving average (SMA) strategy block diagram.

fluctuations in the grid power profile are notably reduced compared to those appearing in the net power profile. As a drawback, without further control, the battery needed to achieve this power profile must have 60 kWh of capacity, which is results too much (in terms of both price and physical size) for a single-family home. As shown in Fig. 5, this capacity arises from the combination of both the expected daily swings but also a seasonal fluctuation. Hence, further improvements in the control strategy are necessary in order to reduce the battery size while maintaining or even enhancing the profile of the power exchanged with the grid.

In order to quantify and compare the quality of the grid power profile in terms of peaks and fluctuations resulting from different energy management strategies, the quality criteria in [37] have been used which are defined as follows:

- Maximum peak (*P+*): Maximum value of the power from the grid during one year (kW);
- Minimum peak (*P−*): Minimum value of the power absorbed from the grid during one year (kW);
- 99 percentile of power peaks (*P99*): 99 percentile of the absolute value of the power profile exchanged with the grid (kW).
- Maximum power derivative (*MPD*): Maximum figure of the absolute value of all power ramps of the grid power profile, evaluated every 15 min, during one year (W/h);
- Average power derivative (*APD*): Average of the absolute value of ramp-rates evaluated every 15 min, of the power exchanged with the grid during one year (W/h);
- Power profile variability (*PPV*): Calculated as the square root of the summation of the squares of the power harmonics of the grid power profile evaluated during a year, divided by the constant component, i.e., the yearly mean power absorbed by the system. Because the energy management strategy does not seek to compensate seasonal variations, which would require much higher energy storage capacity, *PPV* only computes frequencies above 1.65e-06 Hz, i.e., the components with variation periods of one week or less, f_i. moreover, because the sample period is 15 min, the maximum frequency considered to calculate the *PPV* is half the sampling frequency, i.e., the Nyquist frequency, in this case 5.55e-04 Hz, f_f, corresponding to 30–minute variations:

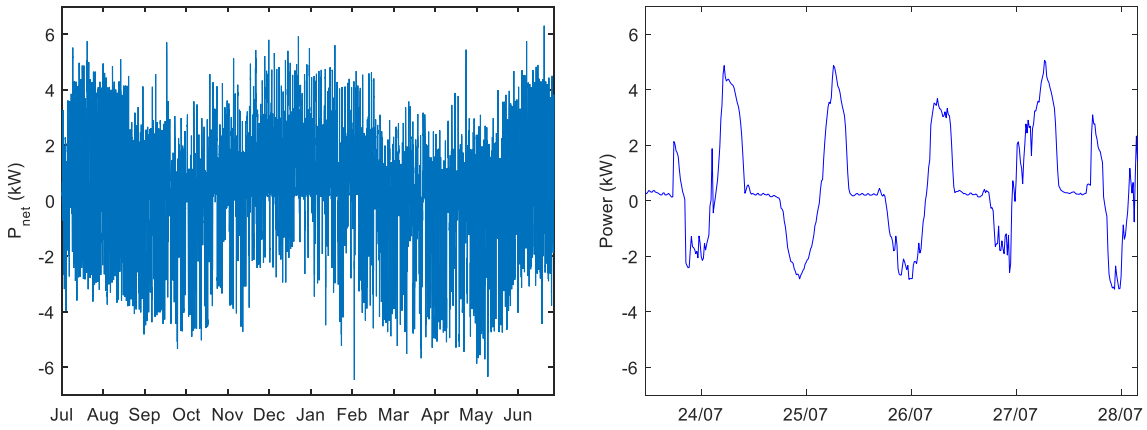

Fig. 2. Net power profile during (a) a year and (b) 4 days of July.

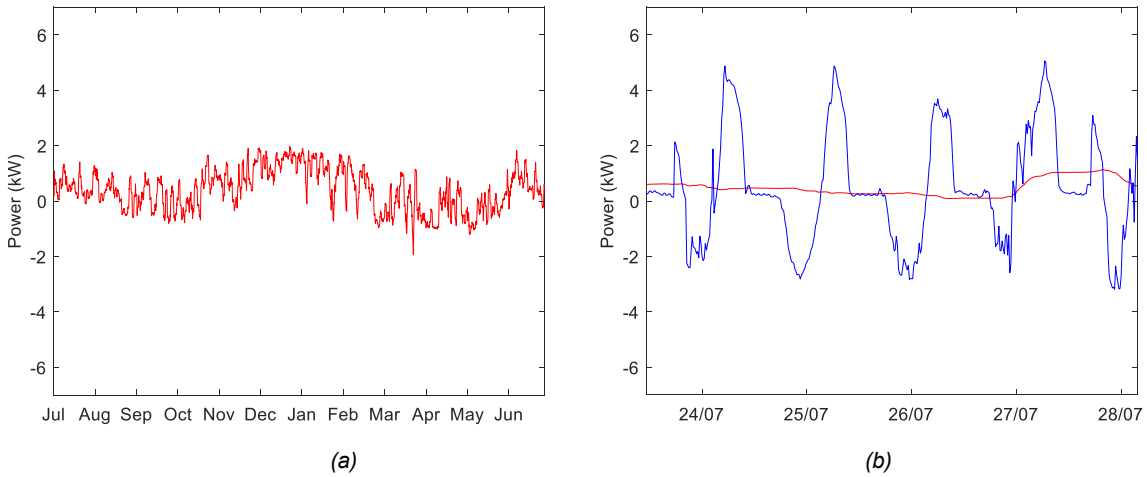

Fig. 4. Power exchanged with the grid using the 24 SMA strategy (a) during a year and (b) during 4 days (red) and net power (blue).

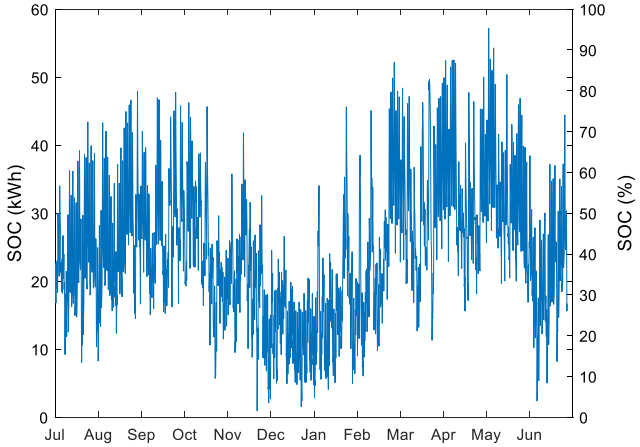

Fig. 5. SOC (in kWh) evolution during a year using the SMA strategy.

$$PPV = \frac{\sqrt{\sum_{f=f_i}^{f_f} P_f^2}}{P_{f=0}}. \quad (3)$$

3. Proposed strategy: power forecasting and DHW subsystem integration

3.1. Strategy overview

The objective of the proposed strategy is to obtain a similar grid power profile to that obtained using the SMA but using a smaller battery than that of previous strategies. This is achieved by combining the idea of using forecasted data and the use of the DHW subsystem resulting in the new proposed algorithm.

Fig. 6 shows a block diagram with the 5 steps of the algorithm and their inputs and outputs. The first two steps are based in the idea of energy balancing in [37] but introducing thermal energy flows and their prediction. As such, in the first step, the grid power is calculated so as to maintain the energy balance in the microgrid. This is achieved by calculating a 24-hour energy balance by using measured and forecasted data of all energy flowing through the boundary of the microgrid. This is then corrected in the second step depending on the forecasting error and the SOC of the battery. In step 3, the heater power is calculated using the energy balance concept but applied only to the DHW water subsystem and, again, corrected for energy imbalances due to forecasting or other sources of error. Steps 4 and 5 use the flexibility of the water heater

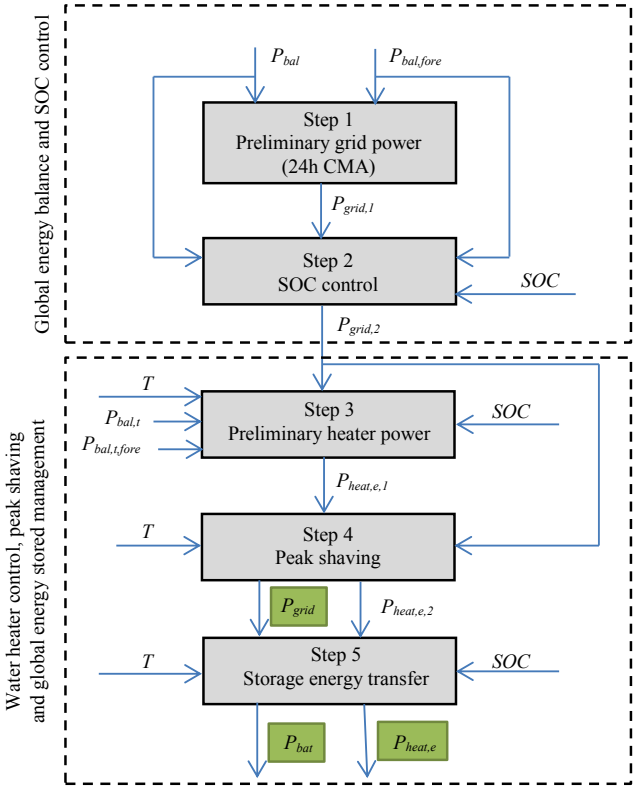

Fig. 6. Proposed strategy algorithm overview.

adding a new step to the control of the SOC of the battery and allowing to absorb renewable power peaks. All 5 steps are briefly described in the following lines and explained in detail in Section 3.2.

In Step 1, the global energy balance of the system is calculated using a 24 h CMA of all powers flowing in and out the system except the grid power. In order to calculate the CMA, data measured from the previous 12 h and forecasted for the next 12 h is used. Regarding consumption forecasting, persistence is used while, for the generation, weather forecasting along with models of the generators is used. However, the value obtained by calculating this CMA is a provisional value for the power to exchange with the grid. This is because the grid power is calculated using predicted values of both consumption and renewable generation, which may have some error.

In fact, if there were some error in the forecasting, as there usually is,

there would be an energy imbalance, which would have to be compensated by the battery, causing undesirable drifts in its desired level of stored energy, even depleting or fully charging the battery. For this reason, the grid power calculated in Step 1 is modified in Step 2 as a function of the SOC and the forecasting error, calculated as the difference between actual and predicted values of the energy balance in the microgrid in the last 3 h.

In Step 3, a provisional power setpoint for the controllable water heater is calculated which comprises two terms. The first term is the CMA of P_{CO} and P_{DHW}, which are the non-controllable energy flows in the DHW node. The second term is proportional to the 24-hour average temperature drift of the hot water tank with respect to a reference value, in order to compensate for errors in the forecasting of powers in the thermal node. These components already eliminate the fluctuations of the hysteresis control in the reference case. Finally, in order to help with the control of the battery SOC, the water heater power calculated is multiplied by a factor proportional to the SOC, so it demands more power when the SOC is higher and less power as it tends to zero. Note that during Step 3 the grid power remains unchanged.

In Step 4, the grid power command is modified if, as a result of the calculations in Step 2, power injected into the grid is above a certain threshold (injection peak-shaving). This is done by diverting part of the power previously assigned to the grid to the electric water heater, which now must absorb more power so it will depend on its temperature. In any case the grid power calculated in this step is the final grid power.

Finally, in Step 5, in case the battery tends towards full charge, and as long as the temperature in the hot water tank is under a certain level, energy is transferred from the battery to the hot water tank by raising the water heater power and the battery delivered by the battery in the same amount, which sets the final power values for the battery and the water heater.

In the next subsection, all 5 steps in the energy management strategy are explained in detail.

3.2. Detailed algorithm

1) Step1: Preliminary grid power calculation for energy balancing

In Step 1, a preliminary grid power setpoint is calculated, $P_{grid,1}$, which aims to compensate the daily energy imbalance in the microgrid (including both the DHW and the electric subsystems). As seen in [37], this energy balancing can be achieved, avoiding fluctuations in the power profile, by computing the moving average of all non-controllable power flows going in and out of the system. In order to also avoid a delay in this action, instead of the SMA, the CMA is used, which needs predicting these power flows for the next 12 h. This value, to be assigned to the grid power, $P_{bal,CMA}$, is computed as follows:

$$P_{grid,1} = P_{bal,CMA} = \frac{1}{24}\left(\int_{t=-12}^{0} P_{bal}dt + \int_{t=0}^{12} P_{bal,fore}dt\right) \quad (4)$$

where the power balance, P_{bal}, is calculated as the difference between power flows going into the system minus power flows going out of the system (excluding the grid power):

$$P_{bal} = P_{con} + P_{DHW} - P_{PV} - P_{WT} - P_{CO}. \quad (5)$$

The calculation of the power balance in the following 12 h is computed as in Eq. (5) except using forecasted values instead of measured values.

In order to forecast PV and wind turbine powers, P_{PV} and P_{WT}, as well as the electric demand, P_{con}, the techniques described in [37] are used, i.e., using weather forecasting and models of the generators in the case of P_{PV} and P_{WT}, and using persistence assuming a 24 h periodicity for the power demand, i.e., for each moment, the predicted consumption power is the power measured 24 h ago. In the proposed strategy hereby presented, the thermal power flows need to be forecasted as well, i.e., the DHW demand and the solar collectors' generation. The DHW demand is forecasted exactly like the electric power demand. Regarding the solar collectors output, it is forecasted by using the weather forecast (solar irradiation and temperature), the efficiency curve given by the manufacturer and persistence for the hot water tank temperature, which is assumed to be the same as the fluid entering the solar collector. Note that, in the common case of not having a measured value for the power output of the solar collector, this forecasting technique can also be used to estimate present values of the solar collector power, only using measured ambient conditions.

To sum up, in Step 1, a grid power setpoint is calculated which, in principle, i.e. if all measurements and forecasting values were flawless, would maintain the global energy balance of the microgrid equal to zero, introducing no drift in the average SOC of the energy storage elements (battery and hot water tank) and with low frequency variations. However, in practice, this calculation would not match real values, mainly due to forecasting errors. The energy imbalance would then be restored by the energy storage elements, hence, making their SOC to drift towards full charge or depletion. In order to correct these undesired deviations, the next step is designed so as to control the SOC, while minimizing the effect over the grid setpoint in terms of peaks and fluctuations.

2) Step 2: SOC control

In Fig. 7.a the net power and its prediction are shown and it can be observed that, as expected, the profiles do not exactly match. The difference between measured and predicted values gather all possible sources of error. These errors may be caused by load forecasting using daily persistence, as seen in the first mismatching peak in Fig. 7.a. Also may be due to errors in the weather forecasting, as seen in the 27th, when there was some sunny hours forecasted for the afternoon but it was finally cloudy (in the experimental results, similar examples are given). And also, the actual error may be due to other factors such as uncertainty in the model of the generators, uncertainty in the efficiency of the battery or inaccurate measurements. In Fig. 7.b the histogram of the hourly total error of the prediction of P_{net} throughout a year is depicted. The error is expressed as a percentage relative to the battery capacity, i.e., as the absolute hourly error, expressed in kWh, divided by the battery capacity, also in kWh. The error lies within ±5% during 90% of the time, which means that most of the time the battery SOC is not compromised by this error. However, the maximum error is 24.9% relative to the battery capacity, meaning it could change its SOC in that amount was it not compensated by the SOC control in this step.

Whichever is the source of the error of the forecasted power profile, in order to avoid that it provokes a full charge or depletion of the storage elements, the grid power setpoint obtained in Step 1, $P_{grid,1}$, is modified by introducing two closed loops for the battery SOC control as shown in Fig. 8, whose output is not only a function of the SOC itself, but also of the prediction error. As it can be observed, the output of each of these loops, namely, P_{SOC} and P_{SOC24}, are added to the value $P_{grid,1}$ resulting in $P_{grid,2}$, which is the preliminary grid power setpoint after Step 2:

$$P_{grid,2} = P_{grid,1} + P_{SOC24} + P_{SOC} \quad (6)$$

The first loop, using a proportional control, brings the 24-hour average of the SOC, SOC_{24h}, to a constant level, *refSOC* established at 50% of the useful SOC of the battery. This is the value around which the instant SOC may vary daily. This first loop, being proportional to the 24 h average of the SOC does not introduce fluctuations of daily frequencies nor higher. The proportionality constant, K_{24}, is set in this case study to 0.025 kW/%, value obtained by performing the dynamic analysis of the system imposing a phase margin of 55° as explained in [37].

On the other hand, the second loop performs a faster control as a function of the instantaneous SOC and the forecasting error. This loop is essential in order to control the SOC instantaneously but, being

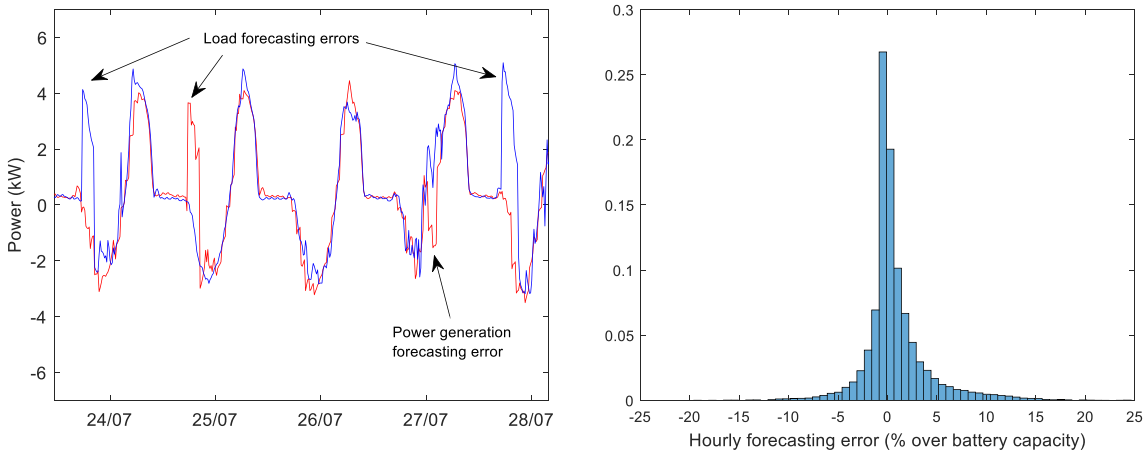

Fig. 7. (a) Pnet (blue) and its prediction (red); (b) histogram of the hourly error expressed in kWh divided by the battery capacity, also in kWh, during a year.

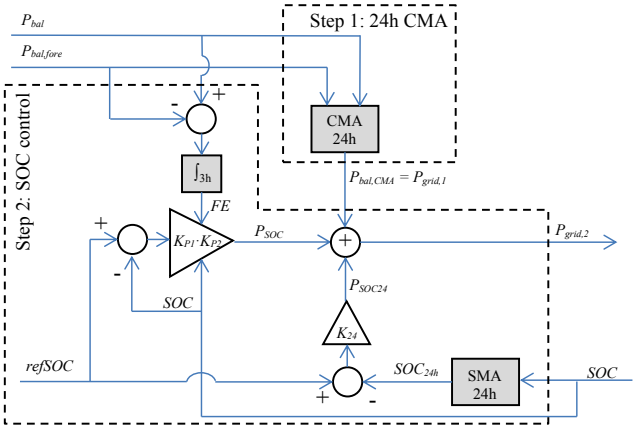

Fig. 8. Preliminary calculation of the grid power setpoint after Step 1 and Step 2.

proportional to the SOC itself, it does introduce fluctuations in the grid power at daily frequencies and higher. For this reason, this instantaneous SOC control loop has been designed so that it is attenuated or even canceled whenever it is not strictly necessary, either because the forecasting error is small or whenever the battery is calculated to be able to cope with the energy imbalance due to the forecasting error. For this control, a new variable, the forecasting error, *FE*, is defined as the difference between the energy balance in the microgrid calculated in the last three hours and its forecasted value. The attenuation of the instantaneous SOC control is achieved by multiplying the SOC error (*refSOC-SOC*) by two factors, K_{P1} and K_{P2} which depend on the SOC itself and *FE*.

In order to obtain the value of K_{P1}, the functions $K_{P1,pos}$ or $K_{P1,neg}$ shown in Fig. 9a (blue and red respectively) are used depending on whether the sign of the forecasting error, *FE*, is positive or negative respectively. These functions take values from zero to a maximum value $K_{P1,max}$, which is fixed for a given scenario; in the case study hereby presented is 0.01 kW/%, as in [37]. For instance, should the forecasting error, *FE*, be positive, i.e., there has been more net consumption than expected in the last three hours, the blue function, $K_{P1,pos}$ is used. In this case, if the battery SOC is above 50%, K_{P1} is set to 0, overriding the instantaneous SOC control in this time-step, as it is considered that the battery has enough energy stored so as to cope with the unforeseen net consumption and the control would let the SOC to evolve down to 50%. If under the same conditions the SOC falls below 50%, a proportional control starts to take action by multiplying the SOC drift (*refSOC-SOC)* by a factor that grows as the SOC approaches 0%. Should the forecast error, *FE*, be negative, a similar but opposite logic would apply, using the red function, $K_{P1,neg}$.

Finally, the action of this control loop is further attenuated by factor K_{P2} which is a function of the forecasting error. As shown in Fig. 9b, if there is no forecasting error, then the factor takes value zero but as the forecasting error grows, the factor K_{P2} grows linearly up to a maximum value of 1 which occurs when the forecasting error, *FE*, represents 25% of the useful capacity of the battery, C_{bat}.

This part of the control is more thoroughly analyzed in [37], where the calculation of every parameter is explained. Finally, Eq. (7) shows how to calculate the preliminary grid power setpoint after Step 2, $P_{grid,2}$:

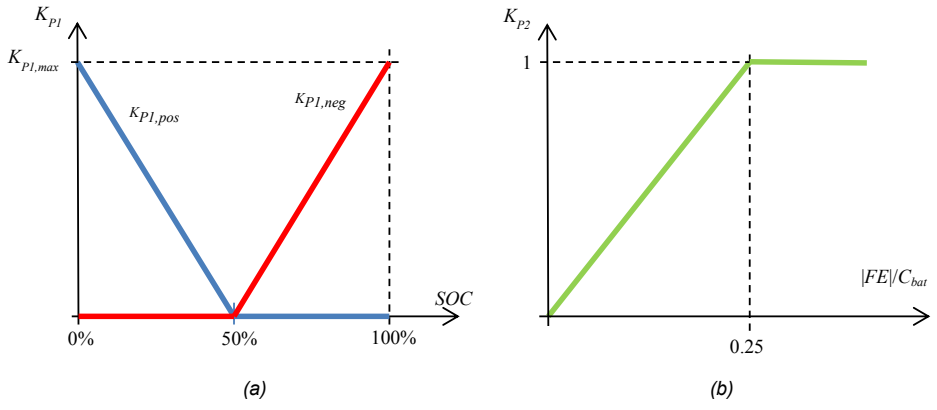

Fig. 9. Functions used to obtain (a) K_{P1} and (b) K_{P2}.

$$P_{grid,2} = P_{grid,1} + K_{24}\cdot(50 - SOC_{24h}) + K_{P1}(SOC, |FE|)\cdot K_{P2}(|FE|)\cdot(50 - SOC) \quad (7)$$

As an example to explain the idea behind this part of the control, Fig. 10 shows, on the top graph, the net power (green) and its prediction (red) along with the SOC of the battery (black) during four days; and on the bottom graph, P_{SOC} (pink) and P_{SOC24} (blue), which are the components added to $P_{grid,1}$ in order to obtain the output variable of Step 2, $P_{grid,2}$. These graphs gather different situations regarding this part of the control, as explained in the following lines. Firstly, during 30th May, an error in solar generation can be observed, while the SOC is below, but close to 50%, hence, P_{SOC} has a low reaction. Therefore, in the first hours after the error, the SOC falls, until P_{SOC24} starts correcting this situation, bringing the SOC again towards the reference, 50%. On the 31st, there is a lower forecasting error and with a somewhat higher SOC, hence, the reaction is now even lower than in the previous day. Moreover, as the SOC lays close to 50% during several hours, P_{SOC24} decreases later on the same day. By the end of the day, the SOC lies around 40%. However, although the SOC remains below 50%, it is not corrected by the instantaneous SOC control as the prediction error is close to zero and it keeps slowly falling despite the average SOC control. Next day, on the 1st June, again, solar generation was expected, but it was finally a cloudy day. Around midday, being the SOC around 30% and having a significant prediction error, unlike previous days, on this day, P_{SOC} highly increases its value preventing the full depletion of the battery before P_{SOC24} can recover the SOC back to around 50% during the following hours and during part of the next day. During the 2nd June, again, there is some prediction error, but as the SOC lies close to 50%, the instantaneous SOC control reacts only smoothly while the average SOC control is highly compensating the energy imbalance of the previous 24 h. Finally, in the evening of the 2nd June, the SOC lies around 30% but, as there is almost no prediction error, the SOC control is mainly composed by the P_{SOC24} component.

3) Step 3: Preliminary water electric heater power for energy balancing

Aiming to keep the water in the hot water tank at around a reference average value, the electric heater feeds to the thermal node the 24 h energy balance of the non-controllable power flows, $P_{bal,t}$, i.e., the difference between the DHW demand and the collectors' power, P_{DHW} and P_{CO}, respectively. Similarly to the global energy balance in Step 1 and for the same reasons, the 24 h CMA is calculated, obtaining $P_{bal,t,CMA}$. Moreover, in order to eliminate accumulated errors in both forecasting and measuring of P_{DHW} and P_{CO}, which would make the temperature of the hot water tank to drift away from its average reference value, another term is added to the power heater setpoint which is proportional to the difference between the temperature reference, 60 °C in the case study, and the 24 h average of the temperature of the hot water tank, P_{T24}. These two terms, $P_{bal,t}$ and P_{T24}, are calculated as follows:

$$P_{balt,CMA} = \frac{1}{24}\left(\int_{t=-12}^{0} P_{bal,t}dt + \int_{t=0}^{12} P_{bal,t,fore}dt\right) \quad (8)$$

$$P_{T24} = K_T\cdot(60 - T_{24h}) \quad (9)$$

where K_T is the control constant of the temperature. The power of the heater is 2 kW so the value of K_T has been set to 1/20 so that in the cases in which temperature reaches its extreme values, this term does not add more than 1 kW. This is an appropriate level for the case study as the maximum daily thermal energy balance in the case study is, expressed as an average power, 0,5 kW.

Moreover, taking advantage of the higher flexibility of the hot water tank, which could (in few occasions) overpass the maximum stablished temperature, and with the objective of helping the battery SOC management, whose restrictions are tighter, a factor is added to the heater power setpoint which is proportional to the SOC of the battery. Whenever the battery SOC is at 50% this factor will be set to 1 and the heater power will be set at ($P_{bal,t,CMA} + P_{T24}$). When the battery SOC changes,

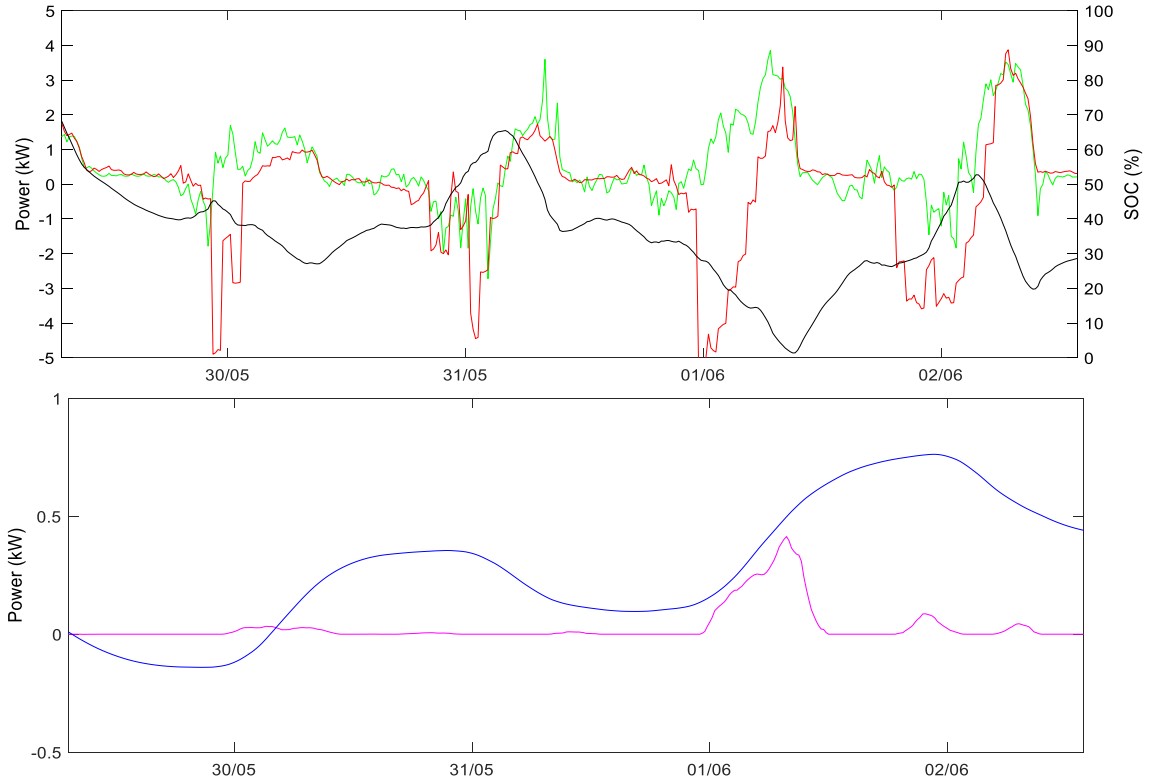

Fig. 10. On the top graph, net power and its prediction (green and red respectively) along with SOC (black) during four days. Bottom graph, P_{SOC} (pink) and P_{SOC24} (blue) for the same four days.

the factor varies linearly down to zero when SOC is zero and up to 2 when SOC is 100%. Thus, the preliminary power setpoint for the heater after Step 3 is calculated as follows:

$$P_{heat,e,1} = \frac{SOC}{50} \cdot (P_{bal,t,CMA} + P_{T24}) \cdot (limited\ to\ 0 \leqslant P_{heat,e,1} \leqslant 2\ \text{kW}) \quad (10)$$

4) Step 4: Injection peak-shaving

Next, in case the calculated grid power, $P_{grid,2}$ implies exchanging power into the grid below a certain threshold, P_{min}, (−1 kW in the case study, and with the sign convention used, where negative means injecting power into the grid) the difference between these two values is diverted to the power heater, as long as the temperature in the hot water tank is below a certain value (70 °C in the case study) and if $P_{heat,e,1}$ is low enough. In the cases where $P_{grid,2}$ is above the threshold value, this step is overridden.

if $T < 70$°C and $P_{grid,2} < P_{min}$	$P_{heat,e,2}=P_{heat,e,1} + (P_{min}-P_{grid,2})$ (with $P_{heat,e} \leq$ 2 kW)	(11.1)
	$P_{grid}= P_{min}$	(11.2)
else	$P_{heat,e,2}=P_{heat,e,1}$	(11.3)
	$P_{grid} = P_{grid,2}$	(11.4)

Note that after this step, the grid power calculated setpoint, P_{grid}, takes its final value, i.e., it is not modified in Step 5.

5) Step 5: Energy storage levelling

Step 5 is aimed at transferring energy within the microgrid, i.e., from the battery to the hot water tank, in order to balance their state of charge. Firstly, given that grid power is already set, the preliminary battery power, $P_{bat,1}$, can be calculated, using the preliminary power setpoint for the water heater as follows:

$$P_{bat,1} = P_{net} - P_{grid} = P_{con} + P_{heat,e,2} - P_{PV} - P_{WT} - P_{grid} \quad (12)$$

However, this value may be changed by changing the electric water heater setpoint. As such, every time the battery SOC tends towards a full charge, which would compromise the manageability of the system, the hot water tank will be used so as to absorb part of the energy in the battery. In order to do so, whenever the battery SOC falls above 90%, the power heater is connected at full power (2 kW in the case study) as long as the temperature in the hot water tank is below a certain value (70 °C in the case study). As a result, power will be demanded from the battery or, at least, the power into the battery will be reduced. In any case, grid power is not altered in this step. The calculations are shown in the following set of equations where power is represented in kW:

if $T < 70$°C and $SOC > 90\%$	$P_{heat,e} = 2$ kW	(13.1)
	$P_{bat}= P_{bat,1} + (2 - P_{heat,e,2})$	(13.2)
else	$P_{heat,e} = P_{heat,e,2}$	(13.3)
	$P_{bat}= P_{bat,1}$	(13.4)

3.3. Simulation results

The algorithm presented is tested by simulation for the case study using a full year of data, resulting in the grid profile shown in Fig. 11a. Fig. 11b shows a close up with the same four days shown in Fig. 2b and Fig. 4b. In this figure, it can be observed how the power profile obtained is notably better in terms of power peaks and fluctuations than the net power and, more importantly, that it is similar to the reference power profile shown in Fig. 4, i.e., the SMA of the net power. Moreover, in Fig. 11a. it can be seen how injection power peaks are limited to a fixed value (1 kW in this case). The success of this strategy lies in an effective way of managing the electric power heater as an active load and in the use of the water tank as energy storage. For instance, thanks to the intelligent control of the water heater, the wide power peaks in the net power profile on the 23th and 27th July shown in Fig. 4b, are eliminated as it can be seen in Fig. 11b. While it is true that some new shorter power peaks do appear in the new net power profile, for example during days 24 to 26 in Fig. 11b, these are, in fact, a result of the battery-heater management, so they do not affect the grid power, but rather help indirectly by relieving the battery SOC. More importantly, all this advantages have come at no cost in terms of end-user comfort as the DHW supply always remains between normal temperature levels.

Moreover, in Fig. 12 it can be observed how with the proposed strategy the battery only undergoes daily fluctuations (and higher frequencies) so that the average SOC remains around 50% throughout the year. Eliminating daily fluctuations or lengthier in the SOC profile (such as those appearing using the SMA strategy, Fig. 5), a better use of the battery is made, hence achieving a similar grid profile than the SMA of the net power yet with a lower battery capacity.

In order to quantify and compare the results, in Table 1, the battery and the quality criteria for the grid power profile are shown for the proposed strategy along with 4 representative reference scenarios. Firstly, we have used as a reference scenario one without a battery and with a common hysteresis control of the heater, i.e., without degrees of freedom, which serves as a worst case scenario in terms of grid power profile, named P_{net} in Table 1. Secondly, as a goal scenario in terms of grid power profile, we use the 24-h moving average of P_{net}, $P_{net,24h}$, which, on the downside, needs a 60 kWh battery. Furthermore, we have

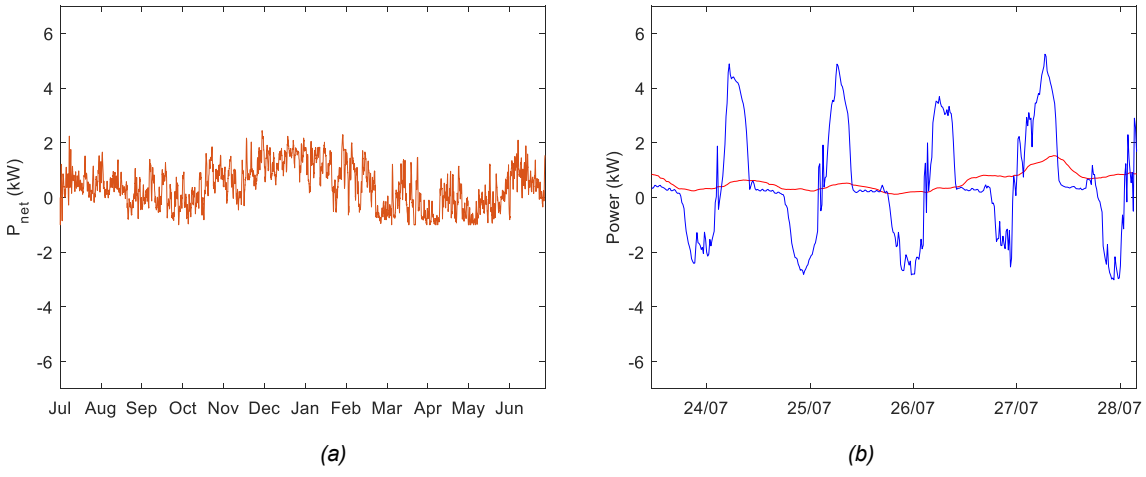

Fig. 11. In red, power exchanged with the grid using the proposed strategy (a) during a year and (b) during four days; in blue, net power.

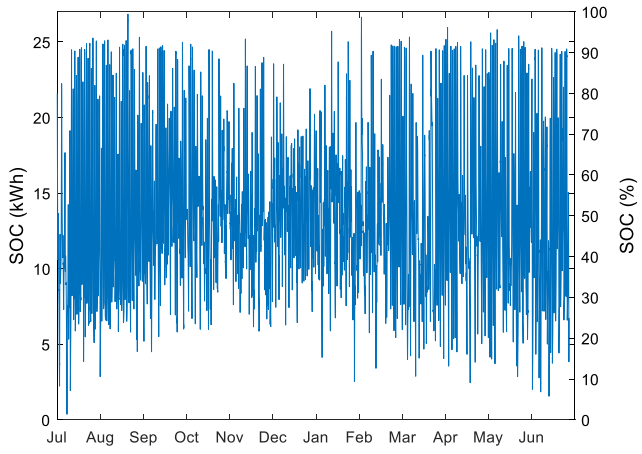

Fig. 12. SOC of the battery throughout the year using the proposed strategy.

added the results of two previous works, updated so as to compare them under the exact same conditions except for the strategy and the battery capacity. These two scenarios allow reducing the battery down to 45 and 36 kWh respectively while keeping a rather smooth grid power profile. Finally, we present the proposed strategy against these four scenarios showing that we have managed to maintain a similar grid power profile while using a battery of only 27 kWh, which is below half the battery capacity used in the second scenario, with the objective power profile. To sum up, the scenarios presented in Table 1 are: (1) net power, (2) 24 h-SMA of net power, (3) grid power applying strategy in [25], (4) grid power applying strategy in [37] and (5) grid power with the proposed strategy.

As it can be observed, quality criteria calculated for the proposed strategy lie close to those obtained with the 24 h-SMA except with a battery capacity 55% smaller. In comparison with strategy in [37] all quality criteria have been notably reduced while using a battery with a capacity that is 25% smaller. Most notably, power peaks, $P+$ and $P-$, have been reduced by 27.1% and 55.1% respectively and *MPD* and *APD* have been reduced by 64.2% and 26.2% respectively. This enhancement is mostly due to the demand management, i.e., the control of the water heater. On the other hand, comparing with strategy in [25], which also uses demand control, not all quality criteria have been reduced, but those lying above, are not much greater while using a battery, which has a capacity 40% smaller. In particular, $P+$ and *P99* are greater by 21% and 8.5%. However, *P-* is lower by 77.5%. Moreover, quality criteria regarding grid power variability, i.e., *MPD*, *APD* and *PPV* have been reduced by 97.3%, 20.1% and 2.2% respectively. To sum up, by using the proposed strategy, which includes demand control and power forecasting, the resulting grid power profile is smoother when compared to all other strategies but using a much lower battery capacity, hence lowering the cost of the system. As the new strategy is compared against a strategy that only uses demand control without power forecasting and another one that uses power forecasting but no demand control, the better results must not only be due to the mere combination of these techniques but to the new strategy needed to combine them. Finally, note that, given the nature of the strategy used, although in a passive way, it already helps with the operation of the grid. Nevertheless, as the strategy has control over the state of charge of the energy storage systems and works with the prediction of the energy state of the microgrid, it is compatible with ancillary services or multimicrogrid environments.

4. Implementation and experimental results

Different energy management strategies can be tested at the Energy Storage and Microgrids Laboratory at UPNA, which is a modular system, as shown in Fig. 13, that can be configured and programmed for any scenario.

The characteristics of the modules of the system are as follow:

- *PV array*. 48 PV modules mounted on the roof, oriented to the south and with an inclination of 30°. They rated power is 4080 W.
- *Small wind turbine*. Bornay INCLIN6000 rated 6 kW is located next to the laboratory at a 20 m height.
- *Battery*. 120 FIAMM SMG300, 2 V, series-connected cells installed in the basement of the laboratory. They have a C_{10} capacity of 300 Ah. Rated capacity thus is 72 kWh, however only 36 kWh are considered useful, so as to keep the depth of discharge (DOD) above 50%, as recommended [42].
- *Programmable electronic load*. Demand profiles can be emulated in real time thanks to AMREL's PLA7.5 K-600–400 electronic load. The load con both reproduce a preset power profile and change the set point in real time following the energy management strategy signals.
- *Power converters*. PV panels, wind turbine and battery power is managed by Ingeteam's INGECON HYBRID MS30 power converter. It is formed by a battery charger, two converters for the wind turbine and the PV panels and a reversible power converter for grid connection. The power to exchange with the grid by the inverter is controlled by the energy management system which sends the set-point every second, while the battery converter balances the power by controlling the voltage of the common DC bus (see Fig. 1a for the architecture).
- *Supervisory and control station*. It is composed by a National Instruments' PXI, a network of sensors and power meters, and a regular PC. Apart from the electrical variables measured by the power meters, the PXI receives every second the data from the sensors network, which comprises a series of 4–20 mA current loops to transmit data from different sensors that measure environmental variables such as temperature, wind speed or irradiance.

The PXI gathers all the data, runs the energy management strategy and sends the setpoints to the inverter and electronic load every second. Moreover, it simulates all the elements not physically present, i.e., the thermal solar collectors and the water tank. The PXI is connected to the PC, which acts as a graphical user interface, i.e., it shows all variables in real time and also serves to send manual signals by the user to the PXI. The PC also runs the programs to check the weather forecast in Meteogalicia's web, converts it to power generation forecast and transmits the data to the PXI. Finally, the PC acts as the database, storing all variables. All programs on the PC and PXI have been developed at UPNA using LabVIEW.

Thanks to this system, the proposed energy management can be tested and analyzed. Firstly, Fig. 14 shows the similarity between the

Table 1
Quality criteria calculated for the net power profile, 24 h-SMA of net power profile and grid power profiles of different strategies with the original battery capacity used in each paper.

Power profile	*Cbat [kWh]*	*P+ [kW]*	*P− [kW]*	*P99 [kW]*	*MPD [W/h]*	*APD [W/h]*	*PPV [–]*
P_{net}	0	6,53	−6,45	4,69	18,648	1222,3	0,361
$P_{net,24h}$	60	1,98	−1,93	1,80	346	33,3	0,071
P_{grid} [25]	45	2,04	−4,45	1,88	21,575	79,1	0,089
P_{grid} [37]	36	3,39	−2,23	2,10	1636	85,6	0,102
P_{grid} *proposed*	27	2,47	−1,00	2,04	586	63,2	0,087

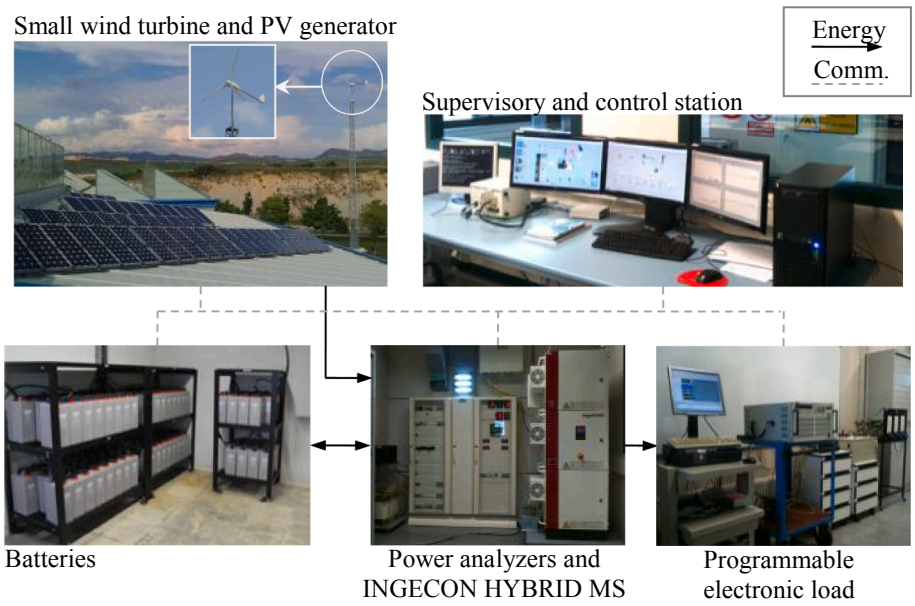

Fig. 13. Microgrid installed at the Public University of Navarre (UPNA).

actual power profiles (red) and the forecasted output (green) for the PV array (top), the solar thermal collectors (second from the top), the wind turbine (second from the bottom) and the loads (bottom). The difference between measured and forecasted power profiles in the case of power generation is mostly due to the weather forecasting uncertainty itself, as it can be seen, for example, in the first two days of PV production in Fig. 14.a. In this case, it was predicted that both days were going to be almost clear. In the end, this was true for the first day, where minor errors still occur due to minor forecasting errors but also due to the model of PV panels and other factors. However, in the second day, the error is mostly due to the fact that it was finally a partially cloudy day when it was predicted to be clear. Note that the forecasted weather data comes from a public, general–purpose server and is used with a 24-h time horizon. If more accuracy is needed, the forecasting error can be reduced by contracting a dedicated weather forecasting provider. However, with the proposed energy management strategy, the error of the forecasting is being compensated, making the extra cost of a dedicated weather forecast server unnecessary.

Fig. 15 shows measured P_{net} (red), forecasted P_{net} (green), measured grid power (solid blue) and calculated grid power by simulation (dashed blue). As can be seen, the profiles of the power exchanged with the grid, both simulated and measured, despite being similar in terms of power peaks and fluctuations, are not exactly equal. The differences between them are mainly due to the SOC estimation; in the simulation, power integration using generic efficiency curves is used while, in the laboratory, the BMS uses its proprietary algorithm. However, the grid profiles are similar in terms of the profile characteristics. As such, it can be said that the strategy works satisfactorily at an energy management level. Nevertheless, the strategy has to be also validated from the point of view of power control, i.e., under rapid power fluctuations.

By looking at a shorter period of time, where rapid power fluctuations can be better appreciated, it can be seen how the system also performs as expected regarding power control. Fig. 16 shows the profiles of the net power (red), battery power (pink) and grid power (blue) along with the SOC of the battery (black) during 30 min on February 26th. As it can be observed, even though the net power fluctuates due to varying solar irradiance, wind gusts and loads, the power exchanged with the grid does not suffer these power swings as the battery absorbs them. Hence, the experimental test shows the good performance of the system from the point of view of the control of the instantaneous power exchanged with the grid.

From the battery point of view, it can be seen that the SOC rises by around 4% during the 30 min period in Fig. 16, as it is absorbing both the excess of generation (negative net power) and the power coming from the grid (set by the strategy to balance the 24-hour energy deficit). Moreover, as it can be observed, despite the battery power fluctuations, the SOC does not show any significant ripple within this 1-second-sampled period of 30 min. Likewise, a simulation working with 15-minutes steps would have accounted for the 4% variation of the SOC but would have overlooked any variations of the SOC within the 15 min time step. However, as these variations have been shown to be neglectible, the 15–minutes time step can be used in the simulations for the energy management analysis.

5. Conclusions

This work presents an energy management strategy reduces power peaks and fluctuations in the grid power profile of an electro-thermal microgrid which comprises renewable generators, electric and thermal consumption and storage in both the electric side and the DHW side which, in turn, are linked together by a controllable electric water heater. The strategy uses its two degrees of freedom (the battery and the combination of an electric water heater and a hot water tank) in order two control the power exchanged with the grid, with a control based on the forecasting of the energetic state of both the electric and the thermal subsystems. The strategy makes use of demand side management by controlling the power absorbed by the electric heater, not only attenuating its own power peaks but absorbing the generation power peaks and helping with the management of the SOC of the battery, hence contributing to a better grid power profile. The simulation of the proposed strategy along with other strategies previously proposed, has proved that the proposed strategy is the best in terms of attenuation of power peaks and fluctuations in the grid power profile. Moreover, the grid power profile is similar to the objective power profile, the 24 h SMA of the net power. And more importantly, this power profile has been achieved with a battery capacity 25% lower than previous strategies. The strategy has also been satisfactorily tested in an experimental microgrid under real conditions.

CRediT authorship contribution statement

Julio Pascual: Conceptualization, Methodology, Software,

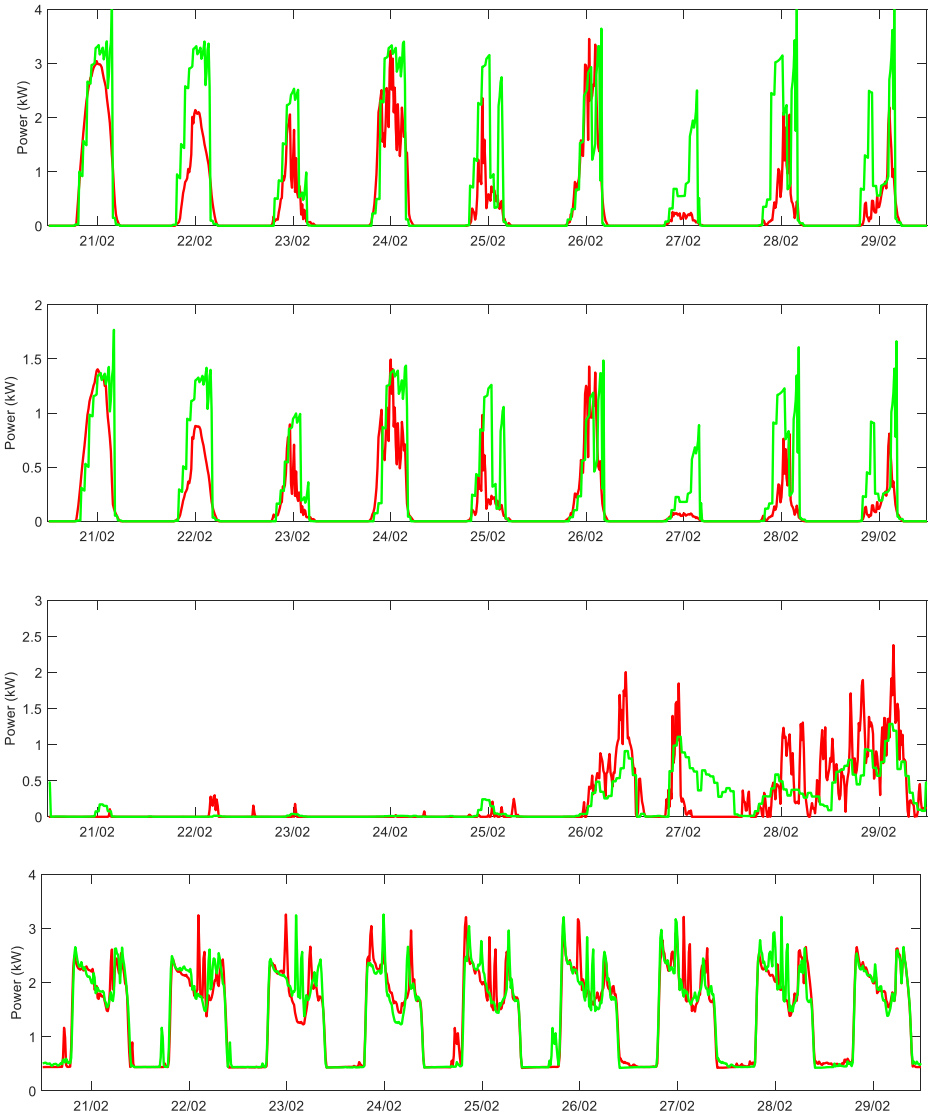

Fig. 14. In red: PV power (top), collectors' power (second from the top), wind power (second from the bottom) and power demand (bottom) during nine days measured at UPNA's microgrid. In green: forecasted values.

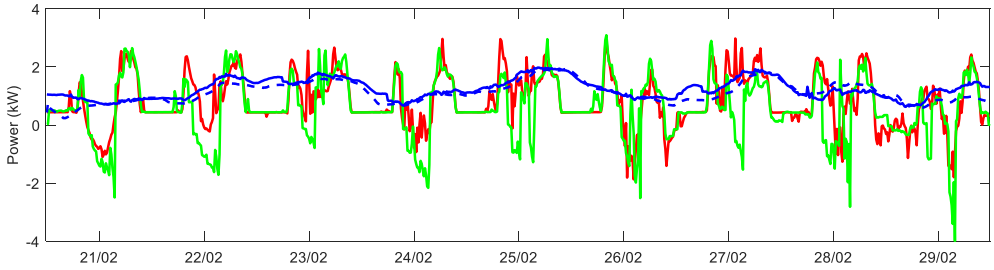

Fig. 15. Measured net power profile (red), forecasted net power profile (green), measured power exchanged with the grid (solid blue) and calculated power exchanged with the grid (dashed blue).

Validation, Formal analysis, Investigation, Data curation, Writing - original draft, Writing - review & editing, Visualization. **Diego Arcos-Aviles:** Conceptualization, Methodology, Software, Validation, Formal analysis, Data curation, Writing - review & editing. **Alfredo Ursúa:** Investigation, Resources, Writing - review & editing, Supervision, Project administration, Funding acquisition. **Pablo Sanchis:** Conceptualization, Methodology, Formal analysis, Investigation, Resources, Writing - review & editing, Supervision, Project administration, Funding acquisition. **Luis Marroyo:** Conceptualization, Methodology, Formal analysis, Investigation, Resources, Writing - original draft, Writing - review & editing, Supervision, Project administration, Funding acquisition.

Declaration of Competing Interest

The authors declare that they have no known competing financial

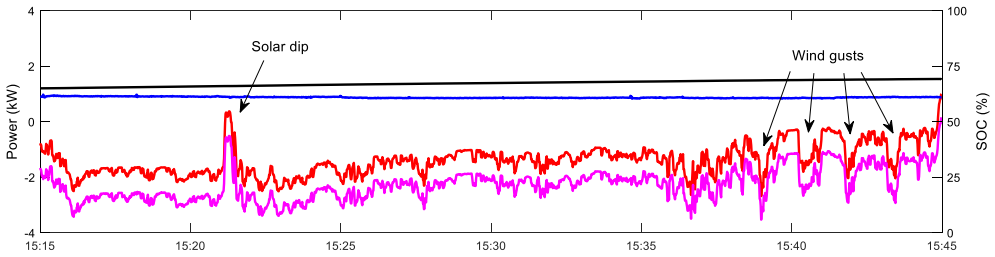

Fig. 16. Net power profile (red), battery power profile (pink), grid power profile (blue) and SOC (black) during 30 min on the 26th February. Despite the power fluctuations of net power, the power exchanged with the grid remains almost constant as the battery absorbs the fluctuations. In addition, the SOC, although gradually changing, does not present any significant ripple within this period.

interests or personal relationships that could have appeared to influence the work reported in this paper.

Acknowledgments

The authors would like to acknowledge that this work has been partially funded under grants PID2019-110816RB-C21 and PID2019–111262RB–I00 by the Spanish State Research Agency (AEI/10.13039/501100011033). And also by VLIR-UOS and the Belgian Development Cooperation (DGD) under the project EC2020SIN322A101 (2020-EXT-007).

References

[1] IEA. World Energy Outlook 2020. Paris: IEA; 2020. ISBN 978-92-64-44923-7.
[2] El-Sharafy MZ, Farag HEZ. Back-feed power restoration using distributed constraint optimization in smart distribution grids clustered into microgrids. Appl Energy 2017;206:1102–17. https://doi.org/10.1016/j.apenergy.2017.08.106.
[3] Janko S, Johnson NG. Reputation-based competitive pricing negotiation and power trading for grid-connected microgrid networks. Appl Energy 2020;277:115598. https://doi.org/10.1016/j.apenergy.2020.115598.
[4] Tuballa ML, Abundo ML. A review of the development of Smart Grid technologies. Renew Sustain Energy Rev 2016;59:710–25. https://doi.org/10.1016/j.rser.2016.01.011.
[5] Industrial C, Utility C, Asmus P, Lawrence M. Executive summary : microgrids analysis and forecasts; 2013.
[6] Schnitzer, D, Lounsbury, DS, Carvallo, JP, Deshmukh, R, Apt, J, Kammen, DM, Microgrids for Rural Electrification : a critical review of best practices based on seven case studies; 2014.
[7] Hatziargyriou N. Microgrids: architectures and control. Chichester, UK: John Wiley & Sons, Ltd; 2014.
[8] Olatomiwa L, Mekhilef S, Ismail MS, Moghavvemi M. Energy management strategies in hybrid renewable energy systems: a review. Renew Sustain Energy Rev 2016;62:821–35. https://doi.org/10.1016/j.rser.2016.05.040.
[9] Xue X, Wang S, Sun Y, Xiao F. An interactive building power demand management strategy for facilitating smart grid optimization. Appl Energy 2014;116:297–310. https://doi.org/10.1016/j.apenergy.2013.11.064.
[10] Comodi G, Giantomassi A, Severini M, Squartini S, Ferracuti F, Fonti A, et al. Multi-apartment residential microgrid with electrical and thermal storage devices: experimental analysis and simulation of energy management strategies. Appl Energy 2015;137:854–66. https://doi.org/10.1016/j.apenergy.2014.07.068.
[11] Velik R, Nicolay P. Grid-price-dependent energy management in microgrids using a modified simulated annealing triple-optimizer. Appl Energy 2014;130:384–95. https://doi.org/10.1016/j.apenergy.2014.05.060.
[12] Tascikaraoglu A, Boynuegri AR, Uzunoglu M. A demand side management strategy based on forecasting of residential renewable sources: a smart home system in Turkey. Energy Build 2014;80:309–20. https://doi.org/10.1016/j.enbuild.2014.05.042.
[13] Niknam T, Azizipanah-Abarghooee R, Narimani MR. An efficient scenario-based stochastic programming framework for multi-objective optimal micro-grid operation. Appl Energy 2012;99:455–70. https://doi.org/10.1016/j.apenergy.2012.04.017.
[14] Chen Y-H, Lu S-Y, Chang Y-R, Lee T-T, Hu M-C. Economic analysis and optimal energy management models for microgrid systems: a case study in Taiwan. Appl Energy 2013;103:145–54. https://doi.org/10.1016/j.apenergy.2012.09.023.
[15] Parisio A, Rikos E, Tzamalis G, Glielmo L. Use of model predictive control for experimental microgrid optimization. Appl Energy 2014;115:37–46. https://doi.org/10.1016/j.apenergy.2013.10.027.
[16] Wang C, Tian T, Xu Z, Cheng S, Liu S, Chen R. Optimal management for grid-connected three/single-phase hybrid multimicrogrids. IEEE Trans Sustainable Energy 2020;11(3):1870–82. https://doi.org/10.1109/TSTE.2019.2945924.
[17] Zadsar M, Sebtahmadi SS, Kazemi M, Larimi SMM, Haghifam MR. Two stage risk based decision making for operation of smart grid by optimal dynamic multi-microgrid. Int J Electr Power Energy Syst 2020;118. https://doi.org/10.1016/j.ijepes.2019.105791.
[18] Chiu WY, Sun H, Vincent Poor H. A multiobjective approach to multimicrogrid system design. IEEE Trans Smart Grid 2015;6(5):2263–72. https://doi.org/10.1109/TSG.2015.2399497.
[19] Cappers P, Goldman C, Kathan D. Demand response in U.S. electricity markets: empirical evidence. Energy 2010;35(4):1526–35. https://doi.org/10.1016/j.energy.2009.06.029. ISSN 0360-5442.
[20] Kim Seul-Ki, Jeon Jin-Hong, Cho Chang-Hee, Ahn Jong-Bo, Kwon Sae-Hyuk. Dynamic modeling and control of a grid-connected hybrid generation system with versatile power transfer. IEEE Trans Ind Electron 2008;55:1677–88. https://doi.org/10.1109/TIE.2007.907662.
[21] Zhou H, Bhattacharya T, Tran D, Siew TST, Khambadkone AM. Composite energy storage system involving battery and ultracapacitor with dynamic energy management in microgrid applications. IEEE Trans Power Electron 2011;26:923–30. https://doi.org/10.1109/TPEL.2010.2095040.
[22] Koohi-Kamali S, Rahim NA, Mokhlis H. Smart power management algorithm in microgrid consisting of photovoltaic, diesel, and battery storage plants considering variations in sunlight, temperature, and load. Energy Convers Manag 2014;84:562–82. https://doi.org/10.1016/j.enconman.2014.04.072.
[23] Barricarte JJ, Martín IS, Sanchis P, Marroyo L. Energy Management strategies for grid integration of microgrids based on renewable energy sources. In: 10th Int. Conf. Sustain. Energy Technol., Istambul, Turkey: 2011, p. 4–7.
[24] Aviles DA, Guinjoan F, Barricarte J, Marroyo L, Sanchis P, Valderrama H. Battery management fuzzy control for a grid- tied microgrid with renewable generation. In: IECON 2012–38th Annu. Conf. IEEE Ind. Electron. Soc. IEEE; 2012. p. 5607–12. https://doi.org/10.1109/IECON.2012.6389008.
[25] Pascual J, Sanchis P, Marroyo L. Implementation and control of a residential electrothermal microgrid based on renewable energies, a hybrid storage system and demand side management. Energies 2014;7:210–37. https://doi.org/10.3390/en7010210.
[26] Marinelli M, Sossan F, Costanzo GT, Bindner HW. Testing of a predictive control strategy for balancing renewable sources in a microgrid. IEEE Trans Sustain Energy 2014;5:1426–33. https://doi.org/10.1109/TSTE.2013.2294194.
[27] Hanna R, Kleissl J, Nottrott A, Ferry M. Energy dispatch schedule optimization for demand charge reduction using a photovoltaic-battery storage system with solar forecasting. Sol Energy 2014;103:269–87. https://doi.org/10.1016/j.solener.2014.02.020.
[28] Masters CL. Voltage rise: the big issue when connecting embedded generation to long 11 kV overhead lines. Power Eng J 2002;16:5–12. https://doi.org/10.1049/pe:20020101.
[29] Mahmud MA, Hossain MJ, Pota HR, Nasiruzzaman ABM. Voltage control of distribution networks with distributed generation using reactive power compensation. In: IECON 2011–37th Annu. Conf. IEEE Ind. Electron. Soc. IEEE; 2011. p. 985–90. https://doi.org/10.1109/IECON.2011.6119329.
[30] Jason W, Black RCL. Strategies to overcome network congestion in infrastructure systems. J Ind Syst Eng 2007;1:97–115.
[31] Parissis O-S, Zoulias E, Stamatakis E, Sioulas K, Alves L, Martins R, et al. Integration of wind and hydrogen technologies in the power system of Corvo island, Azores: a cost-benefit analysis. Int J Hydrogen Energy 2011;36:8143–51. https://doi.org/10.1016/j.ijhydene.2010.12.074.
[32] Shinji T, Sekine T, Akisawa A, Kashiwagi T, Fujita G, Matsubara M. Reduction of power fluctuation by distributed generation in micro grid. Electr Eng Japan 2008;163:22–9. https://doi.org/10.1002/eej.20462.
[33] Arcos-Aviles D, Espinosa N, Guinjoan F, Marroyo L, Sanchis P. Improved fuzzy controller design for battery energy management in a grid connected microgrid. In: IECON 2014–40th Annu. Conf. IEEE Ind. Electron. Soc. IEEE; 2014. p. 2128–33. https://doi.org/10.1109/IECON.2014.7048796.
[34] Sreedharan P, Farbes J, Cutter E, Woo CK, Wang J. Microgrid and renewable generation integration: University of California, San Diego. Appl Energy 2016;169:709–20. https://doi.org/10.1016/j.apenergy.2016.02.053.
[35] Parra D, Walker GS, Gillott M. Are batteries the optimum PV-coupled energy storage for dwellings? Techno-economic comparison with hot water tanks in the UK. Energy Build 2016;116:614–21. https://doi.org/10.1016/j.enbuild.2016.01.039.
[36] Arcos-Aviles D, Vega C, Guinjoan F, Marroyo L, Sanchis P. Fuzzy logic controller design for battery energy management in a grid connected electro-thermal

microgrid. In: 2014 IEEE 23rd Int. Symp. Ind. Electron. IEEE; 2014. p. 2014–9. https://doi.org/10.1109/ISIE.2014.6864926.
[37] Pascual J, Barricarte J, Sanchis P, Marroyo L. Energy management strategy for a renewable-based residential microgrid with generation and demand forecasting. Appl Energy 2015;158:12–25. https://doi.org/10.1016/j.apenergy.2015.08.040.
[38] Arcos-Aviles D, Guinjoan F, Marietta MP, Pascual J, Marroyo L, Sanchis P. Energy management strategy for a grid-tied residential microgrid based on Fuzzy Logic and power forecasting. IECON 2016 - 42nd Annu. Conf. IEEE Ind. Electron. Soc., Florence, Italy: IEEE; 2016, p. 4103–8. doi:10.1109/IECON.2016.7793088.
[39] Arcos-Aviles D, Pascual J, Guinjoan F, Marroyo L, Sanchis P, Marietta MP. Low complexity energy management strategy for grid profile smoothing of a residential grid-connected microgrid using generation and demand forecasting. Appl Energy 2017;205:69–84. https://doi.org/10.1016/j.apenergy.2017.07.123.
[40] Vartiainen E, Masson G, Breyer C, Moser D, Román Medina E. Impact of weighted average cost of capital, capital expenditure, and other parameters on future utility-scale PV levelised cost of electricity. Prog Photovolt Res Appl 2020;28:439–53. https://doi.org/10.1002/pip.3189.
[41] ISO C. What the duck curve tells us about managing a green grid. vol. Fact Sheet; 2012. doi:CommPR/HS/10.2013.
[42] Sauer DU. Electrochemical storage for photovoltaics. Handb. Photovolt. Sci. Eng., Chichester, UK: John Wiley & Sons, Ltd; 2011, p. 896–953. doi:10.1002/9780470974704.ch20.